

See discussions, stats, and author profiles for this publication at: <https://www.researchgate.net/publication/340877805>

# Ca<sup>2+</sup> functions as a molecular switch that controls the mutually exclusive complex formation of pyridoxal phosphatase with CIB1 or Calmodulin

Article in *FEBS Letters* · April 2020

DOI: 10.1002/1873-3468.13795

CITATIONS

0

READS

21

8 authors, including:



**Elisabeth Jeanclos**  
University of Wuerzburg

35 PUBLICATIONS 1,176 CITATIONS

[SEE PROFILE](#)



**Oleg Fedorchenko**  
University of Cologne

14 PUBLICATIONS 198 CITATIONS

[SEE PROFILE](#)



**Andrea Odersky**  
University Hospital Essen

31 PUBLICATIONS 724 CITATIONS

[SEE PROFILE](#)



**Antje Gohla**  
University of Wuerzburg

46 PUBLICATIONS 3,868 CITATIONS

[SEE PROFILE](#)

Some of the authors of this publication are also working on these related projects:



Hematopoietic Protein-1 and the actin cytoskeleton [View project](#)



Neuroblastoma [View project](#)



DR. HERMANN SCHINDELIN (Orcid ID : 0000-0002-2067-3187)

DR. ANTJE GOHLA (Orcid ID : 0000-0002-7442-1487)

Received Date : 18-Mar-2020

Revised Date : 14-Apr-2020

Accepted Date : 15-Apr-2020

Article type : Research Articles

## **Ca<sup>2+</sup> functions as a molecular switch that controls the mutually exclusive complex formation of pyridoxal phosphatase with CIB1 or Calmodulin**

Elisabeth Jeanclos <sup>1,2,a</sup>, Gunnar Knobloch <sup>1,2,b</sup>, Axel Hoffmann <sup>1,2,3</sup>, Oleg Fedorchenko <sup>3,c</sup>,  
Andrea Odersky <sup>3</sup>, Anna-Karina Lamprecht <sup>1,2</sup>, Hermann Schindelin <sup>2</sup>, Antje Gohla <sup>1,2,3,#</sup>

<sup>1</sup> Institute of Pharmacology and Toxicology, University of Würzburg, Germany

<sup>2</sup> Rudolf Virchow Center for Experimental Biomedicine, University of Würzburg, Germany

<sup>3</sup> Institute of Biochemistry and Molecular Biology II, Heinrich Heine University Düsseldorf, Germany

# Correspondence to Antje Gohla, [antje.gohla@uni-wuerzburg.de](mailto:antje.gohla@uni-wuerzburg.de)

<sup>a</sup> Present address: Leibniz Institute for Analytical Sciences ISAS, Dortmund, Germany

<sup>b</sup> Present address: Biomedical Center Munich, Department of Physiological Chemistry, Ludwig-Maximilians-Universität München, Germany

<sup>c</sup> Present address: Department I of Internal Medicine, University Hospital Cologne and Center for Integrated Oncology Cologne-Bonn, Germany

E.J. and G.K. contributed equally to this work

**Running Title:** Ca<sup>2+</sup> controls pyridoxal phosphatase complex formation with CIB1 or CaM

This article has been accepted for publication and undergone full peer review but has not been through the copyediting, typesetting, pagination and proofreading process, which may lead to differences between this version and the [Version of Record](#). Please cite this article as [doi: 10.1002/1873-3468.13795](https://doi.org/10.1002/1873-3468.13795)

This article is protected by copyright. All rights reserved

## ABSTRACT

Pyridoxal 5'-phosphate (PLP) is an essential cofactor for neurotransmitter metabolism. Pyridoxal phosphatase (PDXP)-deficiency in mice increases PLP and  $\gamma$ -aminobutyric acid levels in the brain, yet how PDXP is regulated is unclear. Here, we identify the  $\text{Ca}^{2+}$ - and integrin-binding protein 1 (CIB1) as a PDXP interactor by yeast two-hybrid screening, and found a calmodulin (CaM)-binding motif that overlaps with the PDXP-CIB1 interaction site. Pulldown and crosslinking assays with purified proteins demonstrate that PDXP directly binds to CIB1 or CaM. CIB1 or CaM do not alter PDXP phosphatase activity. However, elevated  $\text{Ca}^{2+}$ -concentrations promote CaM binding and, thereby, diminished CIB1 binding to PDXP, as both interactors bind in a mutually exclusive way. Hence, the PDXP-CIB1 complex may functionally differ from the PDXP- $\text{Ca}^{2+}$ -CaM complex.

## INTRODUCTION

Pyridoxal 5'-phosphate (PLP, active vitamin B6) is a versatile cofactor in the catalysis of numerous biochemical transformations [1]. Mammalian PLP-dependent enzymes drive over 140 different chemical reactions in essential processes such as glucose-, lipid-, amino acid- and neurotransmitter metabolism [2-4]. Sufficient cellular PLP levels are thus critical for a large and important class of enzymes.

In mammals, PLP precursors are taken up by the diet, and PLP is produced by pyridoxal 5'-kinase (PDXK) and pyridox(am)ine 5'-phosphate oxidase (PNPO) [5]. Conversely, intracellular PLP hydrolysis –and thus cofactor inactivation– is catalyzed by the PLP phosphatase PDXP, also known as chronophin [6-10]. Disruptions in vitamin B6 metabolism can lead to disease. For example, insufficient PLP levels in the brain due to inborn errors of vitamin B6 metabolism can cause childhood epilepsy [11] or axonal polyneuropathy with optic atrophy [12]. The PDXK-PLP axis can also be subverted for tumor cell proliferation and maintenance of acute myeloid leukemia [13]. On the other hand, an elevation of intracellular PLP concentrations may be beneficial in neuropsychiatric disorders [14], and to preserve cognitive functions during aging [15].

We have recently demonstrated that PDXP is a major determinant of cellular PLP homeostasis *in vivo* [9]. Whole-body deletion of PDXP in mice strongly increased PLP levels in brain, skeletal muscle and red blood cells. Interestingly, the levels of the major inhibitory neurotransmitter  $\gamma$ -aminobutyric acid (GABA) increased by ~20% in the brains of PDXP knockout mice, whereas the concentrations of dopamine, serotonin, epinephrine and glutamate were unchanged. An altered ratio of excitatory/inhibitory neurotransmission may be involved in the improved spatial learning and memory observed in PDXP knockout mice [9]. While these findings suggest that PDXP is involved in the fine-tuning of GABA levels, the underlying molecular mechanisms are currently unknown.

Information on PDXP regulation is very limited [16,17], and the heat shock protein Hsp90 is the only direct PDXP interactor that has been reported so far [18]. As a first step towards understanding PDXP-dependent cellular processes, we have screened a brain cDNA library for PDXP binding partners. Here, we show that PDXP can directly associate with the  $\text{Ca}^{2+}$ - and integrin-binding protein 1 (CIB1) or with calmodulin (CaM) in a mutually exclusive manner.

CIB1 or CaM did not alter PDXP phosphatase activity *in vitro*. However, we found that Ca<sup>2+</sup> can act as a molecular switch that promotes CaM binding and, thereby, diminishes CIB1 binding to PDXP, as both interactors bind PDXP in a mutually exclusive way. PDXP-CIB1 and PDXP-Ca<sup>2+</sup>-CaM complexes may, therefore, be functionally different. We anticipate that these findings will lay the groundwork for future cellular studies on PDXP-dependent processes in inhibitory neurotransmission.

## RESULTS

### Identification of CIB1 as a PDXP interactor

PDXP is a small phosphatase of the haloacid dehalogenase (HAD) superfamily [8,19] that possesses no apparent protein-protein interaction domains. To identify candidate PDXP interacting proteins, we screened a mouse brain cDNA library using the yeast two-hybrid system. Sixteen different positive clones were obtained, including the previously reported PDXP binding partner Hsp90 [18] (**Table S1**). Two full-length open reading frames coded for the Ca<sup>2+</sup>- and integrin-binding protein 1 (CIB1), a potentially novel PDXP binding partner. CIB1 interacted equally well with PDXP<sup>wt</sup> and with the phosphatase-inactive point mutant PDXP<sup>D25N</sup> [10], indicating that the enzymatic activity of PDXP did not affect the interaction (**Fig. 1A**). CIB1 is an EF hand-containing, broadly expressed protein that can modulate the function and the subcellular localization of diverse effectors, including a number of kinases and the phosphatase calcineurin [20-23]. In the brain, CIB1 has been implicated in the regulation of synaptic plasticity [24], and the protection against stress-induced neurotoxicity [22,25]. Because of these links to physiological and pathological neuronal processes, we decided to characterize the potential CIB1-PDXP interaction in further detail.

To test for a direct interaction between CIB1 and PDXP, we first attached CIB1 to an ELISA plate and incubated with increasing amounts of purified, recombinant PDXP. This type of solid phase binding assay has previously been used to characterize other CIB1 interacting proteins [26,27]. We found that PDXP directly bound to CIB1 in a concentration-dependent and saturable manner (**Fig. 1B**). Subsequently, we performed pulldown experiments with recombinant, purified GST-CIB1 and untagged PDXP. Purified GST was used as a negative control. As shown in the upper panel of **Figure 1C**, PDXP bound to GST-CIB1, but not to GST alone. By densitometrically quantifying the Western blots, we estimated the fraction of PDXP bound to CIB1. With purified proteins, we found a molar ratio of  $\sim 2.5 \times 10^{-3}$  bound PDXP/ total CIB1. We next conducted similar GST-CIB1 *versus* GST pulldown experiments with lysates obtained from HeLa cells expressing exogenous PDXP (**Fig. 1C**, middle panel), and with murine whole brain extracts containing endogenously expressed PDXP (**Fig. 1C**, bottom panel). In both cases, we observed that cellular PDXP specifically bound to immobilized CIB1. In HeLa cell lysates (containing  $\sim 415$  times less PDXP than the reactions in **Fig. 1C** with purified proteins), we found a molar ratio of  $\sim 7.1 \times 10^{-5}$  bound PDXP/total CIB1. In brain whole cell lysates (containing  $\sim 35$  times less PDXP

than the reactions in **Fig. 1C** with purified proteins), we found a molar ratio of  $\sim 4.6 \times 10^{-4}$  bound PDXP/total CIB1. Finally, we tested whether PDXP and CIB1 were also able to interact when both proteins were untagged. HEK293 cells expressing PDXP and/or CIB1 were subjected to immunoprecipitation using a rabbit polyclonal  $\alpha$ -CIB1 antibody. We found that untagged PDXP indeed associated with untagged CIB1 (**Fig. 1D**). Taken together, these results clearly demonstrate a direct interaction between CIB1 and PDXP.

CIB1 contains four EF hands, and its two C-terminal EF hands bind either  $Mg^{2+}$  or  $Ca^{2+}$  (EF-III,  $K_D$  for  $Mg^{2+}$ : 120  $\mu$ M;  $K_D$  for  $Ca^{2+}$ : 1.9  $\mu$ M), or only  $Ca^{2+}$  (EF-IV,  $K_D$  0.5  $\mu$ M) [28]. Metal binding contributes to CIB1 folding, and can thereby affect ligand binding [29,30]. While some CIB1 effectors such as the p21-activated kinase PAK1 show an increased association with CIB1 in the presence of elevated  $[Ca^{2+}]$  [26], a rise in  $[Ca^{2+}]$  reduces binding of the apoptosis signal-regulating kinase ASK1 to CIB1 [22]. Interactors such as  $\alpha$ IIB integrin bind CIB1 in a  $Ca^{2+}$ -independent manner [31-33]. To test the potential effect of reduced or elevated intracellular  $Ca^{2+}$ -levels on the CIB1-PDXP-association, we treated HEK293 cells expressing GST-PDXP and CIB1 with the  $Ca^{2+}$ -chelator BAPTA-AM (**Fig. 1E**) or with the  $Ca^{2+}$ -ionophore A23187 (**Fig. 1F**), and compared the amounts of PDXP-associated CIB1 in GST-sepharose pulldowns. We found that BAPTA-treatment tended to increase the amount of CIB1 in GST-PDXP pulldowns, although this difference was not statistically significant (fold increase of CIB1-PDXP interaction in BAPTA-AM treated cells compared to control cells:  $2.01 \pm 0.59$ , mean values  $\pm$  S.E.M.;  $n=3$ ,  $p=0.163$ , unpaired  $t$ -test). Likewise, we did not detect pronounced changes in the amounts of PDXP-bound CIB1 when cells were treated with A23187 (fold increase of CIB1-PDXP interaction in A23187 treated cells compared to control cells:  $0.83 \pm 0.07$ , mean values  $\pm$  S.E.M.;  $n=3$ ,  $p=0.068$ , unpaired  $t$ -test). These data suggest that the CIB1-PDXP association is largely independent of  $Ca^{2+}$ -concentrations.

### Mapping of the CIB1-PDXP interaction domains

We next set out to identify the domains on PDXP and CIB1 that are involved in their reciprocal binding, and first tested the interaction of N- and C-terminal PDXP truncation mutants with full-length CIB1 in yeast (**Fig. 2A**). **Figure 2B** shows that deletion of the first 80 N-terminal residues of PDXP, which encompass the catalytically essential active site motifs I and II of the phosphatase [10,19], had no detectable effect. However, deletion of five additional amino acids in PDXP<sup>85-292</sup>

abolished the CIB1-PDXP interaction. Consistent with this result, the deletion of more than two-thirds of the PDXP C-terminus up to amino acid 85 was compatible with a CIB1-PDXP interaction. The deletion of five additional amino acids (PDXP<sup>1-80</sup>) reduced the CIB1-PDXP interaction, and the removal of the PDXP C-terminus up to amino acid 75 (PDXP<sup>1-75</sup>) resulted in the loss of a detectable interaction. Together, these data suggest that the region encompassing amino acids 75-85 in PDXP plays an important role in CIB1-PDXP binding. This region consists of a loop and helix H4, is surface-exposed, and located on the back of the active site entrance (**Fig. 2C**). To validate the mapping results, we tested the effect of a 15-amino acid peptide corresponding to residues 76-90 in PDXP on the interaction of full-length, purified CIB1 and PDXP proteins in solid phase binding assays. This peptide (PDXP<sup>76-90</sup>) comprises the mapped CIB1 binding site together with an adjacent strand of  $\beta$ -sheet A and the first three residues of helix H5. **Figure 2D** shows that PDXP<sup>76-90</sup> efficiently competed with CIB1 binding to PDXP. This competition was specific, because it was neither observed in the presence of a scrambled control peptide, nor did PDXP<sup>76-90</sup> impair the CIB1-PAK1 interaction [26].

Crystal [30,34] and solution structures of CIB1 [29,32] show a compact  $\alpha$ -helical protein with extended N- and C-terminal regions, and a hydrophobic channel that is thought to be involved in the binding of CIB1 interactors (**Fig. 3A**). In the absence of a binding partner, this hydrophobic cleft is occluded by helix H10 at the extreme CIB1 C-terminus (amino acids 180-191). Studies with a peptide derived from the high affinity CIB1 interactor  $\alpha$ IIB integrin have demonstrated that the peptide displaces H10, leading to an increased accessibility of the hydrophobic cleft for target binding [35]. In contrast, CD38 (an enzyme that metabolizes cyclic ADP-ribose) can interact with the CIB1 N-terminus [27].

To define the CIB1 domain involved in PDXP binding, we first analyzed the interaction of CIB1 C-terminal truncations with PDXP in yeast (**Fig. 3B**). **Figure 3C** shows that deletion of H10 (designated H13 in the secondary structure plot) in CIB1<sup>1-178</sup> had little effect, whereas the deletion of five additional residues (CIB1<sup>1-173</sup>) strongly diminished the CIB1-PDXP interaction. A complete loss of the CIB1-PDXP interaction was observed upon truncation of the high-affinity Ca<sup>2+</sup>-binding EF hand IV [28], located in between amino acids 161 and 172 (CIB1<sup>1-160</sup>). These data suggest that the C-terminus of CIB1 comprises the PDXP binding region. To test this further, we measured the CIB1-PDXP association in solid phase binding assays. Consistent with the

results obtained in yeast, the binding of PDXP to immobilized full-length CIB1 increased proportionally with the quantity of PDXP until reaching saturation, whereas PDXP showed only residual binding to immobilized CIB1<sup>1-173</sup> (**Fig. 3D**). We conclude that the surface-exposed, C-terminal helices H9 and H10 of CIB1 (corresponding to H12 and H13 in the secondary structure plot in **Fig. 3B**) are important for PDXP binding (**Fig. 3E**).

### **Identification of calmodulin as a binding partner of PDXP and CIB1**

CIB1 is the closest structural homolog of calcineurin B and calmodulin (CaM), two Ca<sup>2+</sup> binding proteins that function as regulatory components of calcineurin A [30]. Calcineurin is a heterodimer, composed of the catalytic A subunit (calcineurin A) that is constitutively bound to the regulatory B subunit (calcineurin B). Ca<sup>2+</sup> binding to calcineurin B results in a small activation of the enzyme, and this basal activity is strongly stimulated by Ca<sup>2+</sup>-CaM binding to calcineurin A [36].

Because PDXP can interact with the calcineurin B homolog CIB1 (albeit in a transient and substoichiometric manner; see **Fig. 1C**), we asked whether PDXP might also bind CaM. Primary sequence analysis of murine PDXP using the Calmodulin Target Database ([calcium.uhnres.utoronto.ca/ctdb/ctdb/home.html](http://calcium.uhnres.utoronto.ca/ctdb/ctdb/home.html)) identified a putative CaM binding motif of the 1-10 subclass with bulky hydrophobic residues spaced eight amino acids apart (<sup>77</sup>FAGLRAEQLF; **Fig. S1A**). Interestingly, the predicted CaM binding site overlaps with the mapped CIB1 binding site on PDXP (amino acids 75-85, see **Fig. 2A**). We also noted a potential CaM binding motif of the 1-8-14 subclass with bulky hydrophobic residues spaced six and five amino acids apart in CIB1 (<sup>21</sup>FLTKQEILLAHRRF; **Fig. S1B, S1C**).

We next performed pulldown assays with purified CaM, PDXP and CIB1 in order to test the potential association of PDXP and CIB1 with CaM experimentally. As shown in **Figure 4A**, both PDXP and CIB1 bound to CaM-sepharose, but not to empty sepharose beads. Since the presumed CaM binding site on PDXP overlaps with the CIB1 binding site, we asked whether CIB1 and CaM would compete for PDXP binding. Indeed, PDXP binding to CaM-beads was reduced in the presence of a ten-fold molar excess of CIB1 over PDXP (**Fig. 4A**). To verify these interactions with endogenous proteins, we used testis tissue lysate as a source of endogenously expressed CIB1

and PDXP. As shown in **Figure 4B**, endogenous PDXP and CIB1 bound to CaM-sepharose in a specific and concentration-dependent manner.

### **Ca<sup>2+</sup> triggers PDXP complex formation with CaM**

CaM is a prototypical Ca<sup>2+</sup> sensor, and proteins with 1-10 and 1-8-14 motifs such as those present in PDXP and CIB1 primarily bind CaM in a Ca<sup>2+</sup>-dependent manner [37]. To investigate the role of Ca<sup>2+</sup> for the binding of CaM to PDXP and CIB1, we assayed the association of purified PDXP and CIB1 with CaM-sepharose under Ca<sup>2+</sup>-free conditions and in the presence of 100 μM Ca<sup>2+</sup>. We observed that the CaM-PDXP association increased, whereas the CIB1-CaM association diminished in the presence of elevated [Ca<sup>2+</sup>]. Likewise, when all three proteins were present, CIB1 competed with PDXP binding to CaM in the absence, but not in the presence of elevated [Ca<sup>2+</sup>] (**Fig. 4C**).

To experimentally test whether the predicted CaM binding site (see **Fig. S1**) indeed overlaps with the mapped CIB1 interaction site on PDXP, we employed the PDXP peptide PDXP<sup>76-90</sup> (see **Fig. 2D**). **Figure 4D** shows that the PDXP<sup>76-90</sup> peptide reduced PDXP binding to CaM sepharose beads. Densitometric analysis showed that PDXP<sup>76-90</sup> reduced the Ca<sup>2+</sup>-CaM-PDXP binding by almost 30% (relative change in Ca<sup>2+</sup>-CaM-PDXP binding compared to scrambled peptide:  $0.72 \pm 0.01$ , data are mean values  $\pm$  S.E.M. in  $n=3$  independent experiments;  $p<0.0001$ , Student's unpaired *t*-test). Higher peptide concentrations such as 10 μM PDXP<sup>76-90</sup> did not lead to a further reduction of Ca<sup>2+</sup>-CaM-PDXP sepharose binding (up to 40 μM PDXP<sup>76-90</sup> were tested with similar results). These data support the predicted 1-10 CaM binding motif, although additional CaM binding sites on PDXP may exist. Taken together, our observations suggest that CIB1, PDXP and CaM can interact in a reciprocal manner in the absence of Ca<sup>2+</sup>, and that elevated [Ca<sup>2+</sup>] favor Ca<sup>2+</sup>-CaM-PDXP complex formation. We have, however, no evidence for the existence of a ternary CaM-CIB1-PDXP complex analogous to the calcineurin holoenzyme.

To further characterize the associations of CIB1 or CaM with PDXP, we performed chemical crosslinking experiments with formaldehyde. Formaldehyde has a short (~2-3 Å) crosslinking span. This enables the detection of protein-protein interactions with high specificity, provided that suitable amino acid residues are present and that formaldehyde can access the binding interface [38]. As shown in the **Supplementary Figure S2**, the incubation of the individual proteins with

formaldehyde did not cause non-specific protein aggregation. Although PDXP exists as a homodimer [6,7,39,40], this dimerization was not stabilized by formaldehyde. **Figure 5A** shows that CIB1-PDXP complexes were readily detectable after crosslinking. CIB1-PDXP binding appeared to be moderately enhanced by the addition of  $\text{Ca}^{2+}$ , but this trend was not statistically significant. These results are consistent with the pulldown experiments shown in **Figures 1E** and **1F**, which indicate that CIB1 and PDXP can already interact in the absence of  $\text{Ca}^{2+}$ , and that this interaction is not markedly increased in the presence of elevated  $\text{Ca}^{2+}$  levels. In contrast, CaM-PDXP crosslinking was barely detectable in the absence of added  $\text{Ca}^{2+}$ , but increased several-fold in the presence of elevated  $[\text{Ca}^{2+}]$ . The same results were obtained when a mixture of CIB1, CaM and PDXP was incubated with formaldehyde in the absence or presence of  $\text{Ca}^{2+}$ , in line with the pulldown experiments shown in **Figure 4C**.

Finally, we examined the CIB1-PDXP and CaM-PDXP crosslinking efficiencies in the presence of all three proteins at different  $[\text{Ca}^{2+}]$ . **Figure 5B** shows that  $[\text{Ca}^{2+}]$  above 20  $\mu\text{M}$  were required to favor CaM-PDXP over CIB1-PDXP complex formation. We note that in the presence of CIB1, the  $\text{Ca}^{2+}$ -induced increase in CaM-PDXP complex formation was attenuated from  $\sim 7$ -fold to  $\sim 2$ -fold compared to CaM-PDXP crosslinking in the absence of CIB1 (see quantifications in **Figs. 5A** and **5B**). These data are in agreement with the observation that CIB1 and  $\text{Ca}^{2+}$ -CaM can compete for PDXP binding (see **Fig. 4C**). Hence, PDXP can engage in complex formation with CIB1 or with CaM, and the latter association is preferred in the presence of  $[\text{Ca}^{2+}]$  above 20  $\mu\text{M}$ .  $[\text{Ca}^{2+}]$  exceeding 20  $\mu\text{M}$  indeed occur physiologically in the brain, *e.g.* in the nanodomains of presynaptic  $\text{Ca}^{2+}$  channels upon channel opening [41].

#### **CIB1 and CaM do not affect PDXP phosphatase activity *in vitro***

CIB1 can directly stimulate or inhibit the activities of kinases such as PAK1 [26] or ASK1 [22], and CaM is a well-known activator of  $\text{Ca}^{2+}$ -CaM-dependent kinases and of the phosphatase calcineurin [42,43]. We therefore examined the potential impact of CIB1 or CaM on the phosphatase activity of PDXP. Using recombinant, purified proteins and pyridoxal 5'-phosphate (PLP) as the physiological PDXP substrate [40], we found that CIB1 and/or CaM had little or no effect on PDXP activity (**Table 1**). Although the presence of 100  $\mu\text{M}$   $\text{Ca}^{2+}$  led to a slight overall increase in the  $K_m$  values and to a decrease in the  $k_{\text{cat}}$  values compared to  $\text{Ca}^{2+}$ -free conditions, this effect can be explained by a competition between the essential cofactor  $\text{Mg}^{2+}$  and catalytically

inert Ca<sup>2+</sup> ions [44]. Thus, the interaction of CIB1 or CaM with PDXP did not alter its phosphatase activity *in vitro*.

Accepted Article

## DISCUSSION

In this work, we report the identification and biochemical characterization of CIB1 and Ca<sup>2+</sup>-CaM as novel PDXP interactors. CaM is a well-characterized activator of the Ca<sup>2+</sup>-dependent phosphatase calcineurin. Interestingly, although the catalytic subunits of calcineurin (calcineurin A) and PDXP are unrelated, they both associate with structurally similar proteins, *i.e.*, with calcineurin B or CIB1. Despite this resemblance, there are important differences in the composition and regulation of the two (holo)enzymes. First, calcineurin A and B subunits form a constitutive heterodimer with basal phosphatase activity. In contrast, the association of PDXP and CIB1 is of low affinity, and PDXP is active in the absence of CIB1 *in vitro* (see below). Second, the binding of Ca<sup>2+</sup>-CaM to calcineurin A results in a full activation of the heterotrimeric enzyme, due to the displacement of an autoinhibitory domain from the catalytic cleft of calcineurin A [36,37,42]. In contrast, Ca<sup>2+</sup>-CaM binding to PDXP was competitive with CIB1, and did not lead to a further activation of the enzyme. Consistent with this finding, no autoinhibitory domains are evident in any of the eight available human or murine PDXP crystal structures (PDB entries 2P27, 2OYC, 2P69, 5AES, 5GYN, 4BX0, 4BX2, 4BX3). Hence, we have no indications for the existence of a PDXP-CIB1-Ca<sup>2+</sup>-CaM holoenzyme analogous to the calcineurin A-calcineurin B-Ca<sup>2+</sup>-CaM heterotrimer. Our results rather suggest that PDXP transiently associates with either CIB1 or Ca<sup>2+</sup>-CaM, as both interactors bind in a mutually exclusive way. As elevated Ca<sup>2+</sup> levels promote CaM binding to PDXP and concomitantly diminish CIB1 binding to PDXP, Ca<sup>2+</sup> appears to function as a molecular switch that can determine the composition of the PDXP complex (Fig. 6). This finding also suggests the possibility that PDXP-CIB1 and PDXP-Ca<sup>2+</sup>-CaM complexes are functionally different.

We did not observe a stimulatory or inhibitory effect of CIB1, CaM or Ca<sup>2+</sup>-CaM on the phosphatase activity of PDXP *in vitro*. Still, it is conceivable that PDXP association with CIB1 or Ca<sup>2+</sup>-CaM affects the subcellular distribution of the phosphatase, and thereby directs its activity to a particular compartment or nanodomain. CIB1 is a myristoylated protein that can be targeted to intracellular membranes or to the plasma membrane *via* its lipid anchor [20]. CIB1 membrane association has been reported to alter the activity of some of its interaction partners. For example, the analysis of CIB1-deficient mouse hearts showed that CIB1 is required to anchor calcineurin B at the sarcolemma [21]. Whereas recombinant, purified CIB1 did not directly induce calcineurin phosphatase activity *in vitro*, CIB1 enhanced cellular calcineurin-NFAT activity through a

Accepted Article

membrane localization-dependent mechanism [21]. It remains to be elucidated if CIB1 (or Ca<sup>2+</sup>-CaM) binding can similarly influence PDXP phosphatase activity in cells.

Further studies on cellular functions of PDXP will likely benefit from the development of experimental tools that allow the visualization of PDXP, CIB1 and CaM at high resolution, ideally at endogenous expression levels, and in living cells. In addition, the development of PLP biosensors to measure PLP levels at subcellular resolution could provide insights into the local regulation of this important cofactor. Exciting progress in this direction has recently been reported [45].

## EXPERIMENTAL PROCEDURES

### Mammalian and bacterial expression constructs

Murine PDXP was reverse transcribed from adult mouse brain cDNA. Total RNA was isolated using TRIzol (Invitrogen) according to the manufacturer's instructions, and cDNA was obtained with the High Fidelity RNA PCR Kit (Takara) and oligo dT primers. The PCR product was subcloned into the *Bam*HI and *Eco*RI restriction sites of pcDNA3 (Invitrogen) to construct untagged PDXP; into the *Kpn*I and *Xho*I sites of pENTR3C (Invitrogen), followed by insertion *via* homologous recombination into pDEST27 (Invitrogen) to produce GST-tagged PDXP for expression in mammalian cells; or into the *Nco*I and *Not*I sites of the bacterial expression vector pETM11 (EMBL) to create N-terminally His<sub>6</sub>-tagged PDXP for *in vitro* studies. Full-length murine CIB1 was PCR-amplified with native Pfu polymerase (Stratagene) using pB42AD-CIB1 as a template. CIB1 was inserted into pcDNA3 *via Eco*RI-*Xho*I to construct untagged CIB1, and into pGEX-4T1 (GE Healthcare) *via Bam*HI-*Xho*I to generate N-terminally tagged GST-CIB1. The C-terminal CIB1 truncation mutant CIB1<sup>1-173</sup> was subcloned from pB42AD (Clontech) into pGEX-4T1 *via Eco*RI-*Xho*I. Murine phosphatase-inactivated PDXP<sup>D25N</sup> was obtained by standard site-directed mutagenesis using Platinum Pfx Polymerase (Invitrogen). CaM cDNA was a kind gift of Dr Atsushi Miyawaki (Brain Science Institute, Wako City, Saitama, Japan) and was cloned in the *Bam*HI/*Xba*I sites of pET3a-1 (Novagen) for expression in *E. coli*, or subcloned in the *Hind*III/*Eco*RI sites of pcDNA3 for mammalian expression. All constructs were verified by sequencing.

### Yeast two-hybrid assays

Library screening was carried out as reported previously [46], using an adult mouse brain cDNA Matchmaker LexA library (Clontech). PDXP<sup>wt</sup> or PDXP<sup>D25N</sup> were subcloned into the *Eco*RI-*Sal*I sites of the modified bait vector pHisLexA/Zeo. This vector was created by introducing the histidine reporter gene *HIS3* into pHybLex/Zeo (Invitrogen). Briefly, pHisLexA/Zeo-PDXP was transformed together with the p8op-*LacZ* reporter gene plasmid into the yeast strain EGY48, followed by transformation with the adult mouse brain cDNA Matchmaker LexA library (Clontech). Co-transformed yeast cells were screened for their ability to grow on selection plates containing 5-bromo-4-chloro-3-indoyl-β-D-galactopyranoside (X-gal), but lacking histidine, tryptophan, uracil and leucine (-H/W/L, +X-gal). Positive clones showing preferential growth and color formation on selection plates with galactose plus raffinose compared to glucose were

identified by sequencing. The CIB1-PDXP-interaction was analyzed by co-transforming the indicated constructs into EGY48. Co-transformants were selected and spotted in parallel onto growth plates (+L, -X-gal) and onto selection plates (-L, +X-gal).

### **Recombinant protein expression and purification**

His<sub>6</sub>-PDXP, GST-CIB1 and CaM were transformed into *E. coli* BL21(DE3) cells (Stratagene), and expressed for 18 h at 20°C (PDXP) or 25°C (CIB1 and CaM) after induction with 0.5 mM isopropyl β-D-thiogalactopyranoside. All purification steps were carried out at 4°C. Transformed cells were harvested by centrifugation for 10 min at 8,000 × g and resuspended in the respective lysis buffers supplemented with protease inhibitors (EDTA-free protease inhibitor tablets, Roche) and 150 U/ml DNase I (Applichem). Cells were lysed using a cell disruptor (Constant Systems Ltd.), and cell debris was removed by centrifugation for 30 min at 30,000 × g.

Untagged PDXP was purified as described [40]. For the purification of recombinant mouse CIB1, bacteria were lysed in 100 mM triethanolamine (TEA), 500 mM NaCl at pH 7.4, and GST-CIB1 was batch-purified on a glutathione sepharose 4B resin (GE Healthcare). After extensive washing with >25 column volumes of wash buffer (50 mM TEA, 250 mM NaCl; pH 7.4), the GST-tag of column-bound CIB1 was cleaved with thrombin (GE Healthcare, 10 U/mL of glutathione sepharose) for 20 h at room temperature. CIB1 was eluted in wash buffer, concentrated and further purified on a HiLoad 16/60 Superdex 200 pg gel filtration column operated on an ÄKTA liquid chromatography system (GE Healthcare) in buffer A (50 mM TEA, 250 mM NaCl, 5 mM MgCl<sub>2</sub>; pH 7.4). For pulldown experiments with immobilized GST-CIB1 (see below), the GST-tag was not cleaved off.

Recombinant, untagged CaM expressing bacteria were lysed in 100 mM TEA, 1 M NaCl, 10 mM CaCl<sub>2</sub> at pH 7.4. Cleared lysates were heat-denatured for 10 min at 80°C, and insoluble material was pelleted by centrifugation for 30 min at 30,000 × g. Cleared supernatants were applied to a phenylsepharose column (Resource PHE, GE Healthcare) in buffer B (50 mM TEA, 1 M NaCl, 10 mM CaCl<sub>2</sub>; pH 7.4), and CaM was eluted in buffer C (50 mM TEA, 250 mM NaCl, 10 mM EGTA; pH 7.4). CaM was further purified on a HiLoad 16/60 Superdex 200 pg size exclusion chromatography column in buffer A. Pure fractions were pooled, concentrated to a protein concentration of 10-20 mg/mL, flash-frozen in liquid nitrogen, and stored at -80°C.

### **Generation of α-CIB1 antibodies**

CIB1-specific rabbit polyclonal antibodies were generated by Charles River using purified full-length murine GST-CIB1 as an immunogen in New Zealand white rabbits, and antibodies were purified by affinity chromatography.

### **Solid phase binding experiments**

Solid phase interaction assays were conducted essentially as described [26]. Ninety-six well microtiter plates were coated overnight at 4°C with 2 µg/well of purified, untagged CIB1 in TMN buffer (40 mM TEA, 30 mM NaCl, 1 mM MgCl<sub>2</sub>; pH 7.4), and nonspecific binding sites were subsequently blocked with 3% protease-free bovine serum albumin (Serva) in TMN buffer for 2 h at room temperature. Wells were incubated for 2 h with purified, untagged PDXP (10 pmol/well), and bound PDXP was detected with rabbit monoclonal α-PDXP antibodies (clone C85E3, Cell Signaling Technology). Subsequently, the wells were incubated for 1 h with horseradish peroxidase-conjugated goat α-rabbit IgG (Pierce). After addition of 3,3',5,5'-tetramethylbenzidine (TMB; Calbiochem) as a horseradish peroxidase substrate, the binding interactions were analyzed continuously by measuring the absorbance at 380 nm or 650 nm.

For peptide competition experiments, the PDXP peptide (C-GFAGLRAEQLFSSAL) or the control peptide (C-LALQGFSRSLNAFAG, both custom-synthesized by Anaspec Inc. with >95% purity and employed at 50 - 1000 pmol/well) were incubated in TMN buffer with the pre-coated CIB1 for 1 h. Afterwards, purified, untagged PDXP or purified human PAK1 protein (Biaffin GmbH) was added for 2 h. Wells were incubated with α-PDXP or α-PAK1/2/3 antibodies (both from Cell Signaling Technology), and bound proteins were measured as described above.

### **Cell culture, pulldown assays and co-immunoprecipitation**

HeLa cells (American Type Culture Collection) and HEK293-AD cells (referred to as HEK293 cells; Stratagene) were cultured in Dulbecco's modified Eagle's medium (DMEM) containing 10% fetal calf serum (FCS), 2 mM L-glutamine, 100 U/mL penicillin and 100 µg/mL streptomycin.

For pulldown experiments with isolated proteins, purified GST or GST-CIB1 were incubated with untagged PDXP (~5 µg of each protein) for 2 h at 4°C under rotation in pulldown buffer (40 mM TEA, 30 mM NaCl, 1 mM MgCl<sub>2</sub>, 0.1% Triton X-100, 1 mM β-mercaptoethanol, 1 µg/mL aprotinin, 1 µg/mL leupeptin, 1 µg/mL pepstatin; pH 7.4).

For pulldown experiments with exogenously expressed PDXP, HeLa cells were transfected with 0.2  $\mu$ g pcDNA3-PDXP or vector DNA and 3  $\mu$ L of LipofectAmine 2000 in OptiMEM (both Invitrogen) per well of a 6-well plate. After 16 h, cells were scraped in pulldown buffer and lysed by passing through a 24-gauge needle on ice. Unbroken material and cellular debris were removed by centrifugation (12,000  $\times$  g, 15 min, 4°C), and the protein concentration of the clarified lysates was determined using the Micro BCA assay (Pierce). For each sample, an aliquot corresponding to 300  $\mu$ g of total protein was incubated with 5  $\mu$ g of immobilized GST or GST-CIB1 for 4 h under rotation at 4°C. For pulldown experiments with endogenously expressed PDXP, one adult mouse brain was minced in pulldown buffer and lysed as described above. Three hundred  $\mu$ g of the whole brain lysate were incubated with 5  $\mu$ g of immobilized GST or GST-CIB1 for 4 h at 4°C under rotation. In all cases, the beads were collected by centrifugation and washed three times in pulldown buffer. The associated proteins were resolved by SDS-PAGE and blotted onto nitrocellulose membranes (Hybond C, Amersham). PDXP binding to CIB1 was assessed by Western blot analysis with PDXP-specific antibodies.

To assess the effect of calcium on the CIB1-PDXP interaction in cells, HEK293 cells were seeded in 10 cm dishes (2-3 $\times$ 10<sup>6</sup> cells/dish). On the next day, cells were transfected with CIB1 (in pcDNA3) and either GST or GST-PDXP (in pDEST27) using TransIT-LT1 (Mirus Bio). Twenty hours after transfection, cells were serum-starved for 16 h in DMEM (containing 2 mM Ca<sup>2+</sup>), treated with 5  $\mu$ M of the calcium ionophore A23187 (Calbiochem) or with the vehicle DMSO for 3 min, briefly rinsed in TMN (30 mM TEA, 150 mM NaCl, 1 mM MgCl<sub>2</sub>; pH 7.5) prewarmed to 37°C, and then lysed by shear stress (10 passages through a 25G  $\times$  5/8" syringe) at 4°C in interaction buffer (TMN containing 1 mM DTT, 5  $\mu$ g/mL aprotinin, 1  $\mu$ g/mL pepstatin, 1  $\mu$ g/mL leupeptin, 1 mM pefabloc, and supplemented with 1 mM CaCl<sub>2</sub> for cells treated with A23187). After centrifugation at 15,000  $\times$  g for 15 min at 4°C, the lysates were incubated for 1 h under constant rotation with glutathione beads (pre-equilibrated in interaction buffer supplemented with 3% (w/v) bovine serum albumin) at room temperature. The beads were washed four times with TMN (supplemented with 1 mM DTT  $\pm$  CaCl<sub>2</sub>) using a vacuum manifold; bead-associated proteins were eluted with Laemmli's sample buffer, and the eluates were analyzed on a 12% SDS-PAGE gel and immunoblotted against PDXP or CIB1. To analyze the effect of reduced cellular Ca<sup>2+</sup> levels on the CIB1-PDXP interaction, cells were seeded and transfected as described above. Twenty hours after transfection, cells were washed once in Hank's Balanced Salt Solution

(HBSS). Cells were then incubated for 30 min in HBSS containing 20  $\mu\text{M}$  of the cell-permeable  $\text{Ca}^{2+}$ -chelator BAPTA-AM (Molecular Probes/Invitrogen) or the DMSO solvent control. Cells were rinsed and lysed in TMN as described above, except that the TMN lysis buffer was supplemented with 5 mM EGTA for BAPTA-treated cells, and with 1 mM  $\text{CaCl}_2$  for DMSO control-treated cells. Lysates were then processed as described above, and beads were washed as described except that the TMN washing buffer was supplemented with 1 mM DTT and additionally with 5 mM EGTA for BAPTA-treated cells, or with 1 mM  $\text{CaCl}_2$  for control treated cells. Bead-associated proteins were eluted with Laemmli's sample buffer, and eluates were analyzed on a 12% SDS-PAGE gel and immunoblotted against PDXP or CIB1.

For co-immunoprecipitation experiments, HEK293 cells were seeded in 3.5 cm wells ( $4.5 \times 10^5$  cells/well) and transfected with untagged murine pcDNA3-PDXP, alone or in combination with untagged murine pcDNA3-CIB1. The amount of transfected plasmid DNA was kept constant with pcDNA3 empty vector. Cells were lysed as described above in interaction buffer (without DTT); lysates were incubated with  $\alpha$ -CIB1 antibodies for 1 h at  $4^\circ\text{C}$ , and protein A beads (GE Healthcare) were used for immunoprecipitation.

For pulldown assays with CaM, sepharose-immobilized CaM (GE Healthcare) was equilibrated in HNT buffer (20 mM HEPES, 100 mM NaCl, 0.1% Triton X-100; pH 7.4) supplemented with 5 mM EGTA or 100  $\mu\text{M}$   $\text{CaCl}_2$ . PDXP (14.5 ng) and/or CIB1 (100 ng; corresponding to a molar ratio of 1:10) were incubated with 50  $\mu\text{L}$  of CaM sepharose beads for 90 min at  $4^\circ\text{C}$  under rotation. As a bead control, sepharose (GE Healthcare) was inactivated using Tris base. Beads were washed three times in wash buffer (20 mM HEPES, 500 mM NaCl, 1% Triton X-100; pH 7.4), and associated proteins were solubilized in Laemmli's buffer, separated by SDS-PAGE and analyzed by probing with CIB1- or PDXP-specific antibodies. For pulldown assays of endogenously expressed CIB1 or PDXP, one rat testis was homogenized in 5 mL of ice-cold HNT buffer supplemented with protease inhibitors (5  $\mu\text{g}/\text{mL}$  aprotinin, 1  $\mu\text{g}/\text{mL}$  pepstatin, 1  $\mu\text{g}/\text{mL}$  leupeptin, 1 mM PMSF) using a Dounce homogenizer. Unbroken material and cell debris were removed by centrifugation, and 1 mL of the cleared lysate was added to 50  $\mu\text{L}$  CaM sepharose (or to an equal volume of inactivated sepharose control beads) per reaction. Samples were incubated overnight at  $4^\circ\text{C}$  under constant rotation. Subsequently, beads were washed three times in wash buffer and processed for Western blot analysis as described above.

For peptide competition assays, CaM-sepharose was equilibrated in HNT buffer supplemented with 100  $\mu\text{M}$   $\text{CaCl}_2$ . Fifty  $\mu\text{L}$  CaM sepharose or Tris-inactivated sepharose control

beads (see above) were pre-incubated for 60 min at 4°C under rotation with the indicated concentrations of the PDXP<sup>76-90</sup> peptide or the scrambled control peptide (see above under solid phase binding experiments). Afterwards, PDXP (14.5 ng, or 0.44 pmol) was added for 90 min at 4°C under rotation. Beads were washed three times in wash buffer supplemented with 100 µM CaCl<sub>2</sub>, and associated proteins were solubilized in Laemmli's buffer, separated by SDS-PAGE and analyzed with PDXP-specific antibodies.

### **Crosslinking experiments**

Five µM of PDXP was incubated for 2 h at 37°C with 10 µM of CIB1 and/or 10 µM of CaM (all proteins were untagged) in a total volume of 15 µL in buffer A supplemented with 50 µM EGTA ± different concentrations of CaCl<sub>2</sub> and 0.67% formaldehyde. Crosslinking was stopped by the addition of Laemmli's sample buffer, and proteins were resolved by SDS-PAGE and stained with Coomassie Brilliant Blue. Band intensities were analyzed densitometrically using the software ImageJ, version 1.44 (<http://rsb.info.nih.gov/ij/>).

### ***In vitro* phosphatase assays**

One hundred nM of PDXP were pre-incubated in the absence or presence of 1 µM CIB1 or 1 µM CaM (all proteins were untagged) for 10 min at 22°C in buffer A supplemented with 0.001% Triton X-100 and 1 mM EGTA or 100 µM CaCl<sub>2</sub> at pH 7.4. The reactions were started by the addition of PLP (final concentrations ranging from 0 – 500 µmol/L in a total volume of 50 µL), and stopped after 2 min by the addition of 100 µL Biomol Green (Enzo Life Sciences). Color was allowed to develop for 10 min and the absorbance of the resulting phosphomolybdate complex was read at 620 nm on an Envision 2104 multilabel microplate reader (Perkin Elmer). Free phosphate release was quantitated using phosphate standard curves, and  $v_{max}$  and  $K_m$  were calculated using GraphPad Prism, version 4.01.

### **Statistical analysis**

Statistically significant differences were analyzed using Student's unpaired, two-tailed *t*-tests, using GraphPad Prism version 7.05. Statistically significant differences in the effect of Ca<sup>2+</sup> on CIB1-PDXP or CaM-PDXP-complex formation were analyzed with the Mann-Whitney two-tailed test, using GraphPad Prism version 4.01.

## REFERENCES

- [1] Richard, J.P., Amyes, T.L., Crugeiras, J. and Rios, A. (2009). Pyridoxal 5'-phosphate: electrophilic catalyst extraordinaire. *Curr Opin Chem Biol* 13, 475-83.
- [2] Percudani, R. and Peracchi, A. (2003). A genomic overview of pyridoxal-phosphate-dependent enzymes. *EMBO Rep* 4, 850-4.
- [3] Eliot, A.C. and Kirsch, J.F. (2004). Pyridoxal phosphate enzymes: mechanistic, structural, and evolutionary considerations. *Annu Rev Biochem* 73, 383-415.
- [4] Fux, A., Pfanzelt, M., Kirsch, V.C., Hoegl, A. and Sieber, S.A. (2019). Customizing Functionalized Cofactor Mimics to Study the Human Pyridoxal 5'-Phosphate-Binding Proteome. *Cell Chem Biol* 26, 1461-1468 e7.
- [5] di Salvo, M.L., Contestabile, R. and Safo, M.K. (2011). Vitamin B(6) salvage enzymes: mechanism, structure and regulation. *Biochim Biophys Acta* 1814, 1597-608.
- [6] Fonda, M.L. (1992). Purification and characterization of vitamin B6-phosphate phosphatase from human erythrocytes. *J Biol Chem* 267, 15978-83.
- [7] Jang, Y.M., Kim, D.W., Kang, T.C., Won, M.H., Baek, N.I., Moon, B.J., Choi, S.Y. and Kwon, O.S. (2003). Human pyridoxal phosphatase. Molecular cloning, functional expression, and tissue distribution. *J Biol Chem* 278, 50040-6.
- [8] Gohla, A. (2019). Do metabolic HAD phosphatases moonlight as protein phosphatases? *Biochim Biophys Acta Mol Cell Res* 1866, 153-166.
- [9] Jeanclos, E. et al. (2019). Improved cognition, mild anxiety-like behavior and decreased motor performance in pyridoxal phosphatase-deficient mice. *Biochim Biophys Acta Mol Basis Dis* 1865, 193-205.
- [10] Gohla, A., Birkenfeld, J. and Bokoch, G.M. (2005). Chronophin, a novel HAD-type serine protein phosphatase, regulates cofilin-dependent actin dynamics. *Nat Cell Biol* 7, 21-9.
- [11] Wilson, M.P., Plecko, B., Mills, P.B. and Clayton, P.T. (2019). Disorders affecting vitamin B6 metabolism. *J Inherit Metab Dis* 42, 629-646.
- [12] Chelban, V. et al. (2019). PDXK mutations cause polyneuropathy responsive to pyridoxal 5'-phosphate supplementation. *Ann Neurol* 86, 225-240.
- [13] Chen, C.C. et al. (2020). Vitamin B6 Addiction in Acute Myeloid Leukemia. *Cancer Cell* 37, 71-84 e7.
- [14] di Salvo, M.L., Safo, M.K. and Contestabile, R. (2012). Biomedical aspects of pyridoxal 5'-phosphate availability. *Front Biosci (Elite Ed)* 4, 897-913.

- [15] Jannusch, K., Jockwitz, C., Bidmon, H.J., Moebus, S., Amunts, K. and Caspers, S. (2017). A Complex Interplay of Vitamin B1 and B6 Metabolism with Cognition, Brain Structure, and Functional Connectivity in Older Adults. *Front Neurosci* 11, 596.
- [16] Delorme-Walker, V., Seo, J.Y., Gohla, A., Fowler, B., Bohl, B. and DerMardirossian, C. (2015). Chronophin coordinates cell leading edge dynamics by controlling active cofilin levels. *Proc Natl Acad Sci U S A* 112, E5150-9.
- [17] Zoudilova, M., Min, J., Richards, H.L., Carter, D., Huang, T. and DeFea, K.A. (2010). beta-Arrestins scaffold cofilin with chronophin to direct localized actin filament severing and membrane protrusions downstream of protease-activated receptor-2. *J Biol Chem* 285, 14318-29.
- [18] Huang, T.Y., Minamide, L.S., Bamburg, J.R. and Bokoch, G.M. (2008). Chronophin mediates an ATP-sensing mechanism for cofilin dephosphorylation and neuronal cofilin-actin rod formation. *Dev Cell* 15, 691-703.
- [19] Seifried, A., Schultz, J. and Gohla, A. (2013). Human HAD phosphatases: structure, mechanism, and roles in health and disease. *FEBS J* 280, 549-71.
- [20] Leisner, T.M., Freeman, T.C., Black, J.L. and Parise, L.V. (2016). CIB1: a small protein with big ambitions. *FASEB J* 30, 2640-50.
- [21] Heineke, J. et al. (2010). CIB1 is a regulator of pathological cardiac hypertrophy. *Nat Med* 16, 872-9.
- [22] Yoon, K.W. et al. (2009). CIB1 functions as a Ca(2+)-sensitive modulator of stress-induced signaling by targeting ASK1. *Proc Natl Acad Sci U S A* 106, 17389-94.
- [23] Zhu, W. et al. (2017). CIB1 contributes to oncogenic signalling by Ras via modulating the subcellular localisation of sphingosine kinase 1. *Oncogene* 36, 2619-2627.
- [24] Kauselmann, G. et al. (1999). The polo-like protein kinases Fnk and Snk associate with a Ca(2+)- and integrin-binding protein and are regulated dynamically with synaptic plasticity. *EMBO J* 18, 5528-39.
- [25] Yoon, K.W. et al. (2017). CIB1 protects against MPTP-induced neurotoxicity through inhibiting ASK1. *Sci Rep* 7, 12178.
- [26] Leisner, T.M., Liu, M., Jaffer, Z.M., Chernoff, J. and Parise, L.V. (2005). Essential role of CIB1 in regulating PAK1 activation and cell migration. *J Cell Biol* 170, 465-76.
- [27] Liu, J. et al. (2017). Cytosolic interaction of type III human CD38 with CIB1 modulates cellular cyclic ADP-ribose levels. *Proc Natl Acad Sci U S A* 114, 8283-8288.

- [28] Yamniuk, A.P., Nguyen, L.T., Hoang, T.T. and Vogel, H.J. (2004). Metal ion binding properties and conformational states of calcium- and integrin-binding protein. *Biochemistry* 43, 2558-68.
- [29] Yamniuk, A.P., Silver, D.M., Anderson, K.L., Martin, S.R. and Vogel, H.J. (2007). Domain stability and metal-induced folding of calcium- and integrin-binding protein 1. *Biochemistry* 46, 7088-98.
- [30] Gentry, H.R., Singer, A.U., Betts, L., Yang, C., Ferrara, J.D., Sondek, J. and Parise, L.V. (2005). Structural and biochemical characterization of CIB1 delineates a new family of EF-hand-containing proteins. *J Biol Chem* 280, 8407-15.
- [31] Yamniuk, A.P. and Vogel, H.J. (2005). Calcium- and magnesium-dependent interactions between calcium- and integrin-binding protein and the integrin alphaIIb cytoplasmic domain. *Protein Sci* 14, 1429-37.
- [32] Huang, H., Ishida, H., Yamniuk, A.P. and Vogel, H.J. (2011). Solution structures of Ca<sup>2+</sup>-CIB1 and Mg<sup>2+</sup>-CIB1 and their interactions with the platelet integrin alphaIIb cytoplasmic domain. *J Biol Chem* 286, 17181-92.
- [33] Huang, H. and Vogel, H.J. (2012). Structural basis for the activation of platelet integrin alphaIIbbeta3 by calcium- and integrin-binding protein 1. *J Am Chem Soc* 134, 3864-72.
- [34] Blamey, C.J., Ceccarelli, C., Naik, U.P. and Bahnson, B.J. (2005). The crystal structure of calcium- and integrin-binding protein 1: insights into redox regulated functions. *Protein Sci* 14, 1214-21.
- [35] Yamniuk, A.P., Ishida, H. and Vogel, H.J. (2006). The interaction between calcium- and integrin-binding protein 1 and the alphaIIb integrin cytoplasmic domain involves a novel C-terminal displacement mechanism. *J Biol Chem* 281, 26455-64.
- [36] Klee, C.B., Ren, H. and Wang, X. (1998). Regulation of the calmodulin-stimulated protein phosphatase, calcineurin. *J Biol Chem* 273, 13367-70.
- [37] Chin, D. and Means, A.R. (2000). Calmodulin: a prototypical calcium sensor. *Trends Cell Biol* 10, 322-8.
- [38] Nadeau, O.W. and Carlson, G.M. (2007). Protein Interactions Captured by Chemical Cross-linking: One-Step Cross-linking with Formaldehyde. *CSH Protoc* 2007, pdb prot4634.
- [39] Almo, S.C. et al. (2007). Structural genomics of protein phosphatases. *J Struct Funct Genomics* 8, 121-40.

- [40] Kestler, C., Knobloch, G., Tessmer, I., Jeanclos, E., Schindelin, H. and Gohla, A. (2014). Chronophin dimerization is required for proper positioning of its substrate specificity loop. *J Biol Chem* 289, 3094-103.
- [41] Wu, L.G., Hamid, E., Shin, W. and Chiang, H.C. (2014). Exocytosis and endocytosis: modes, functions, and coupling mechanisms. *Annu Rev Physiol* 76, 301-31.
- [42] Rusnak, F. and Mertz, P. (2000). Calcineurin: form and function. *Physiol Rev* 80, 1483-521.
- [43] Liu, J.O. (2009). Calmodulin-dependent phosphatase, kinases, and transcriptional corepressors involved in T-cell activation. *Immunol Rev* 228, 184-98.
- [44] Peeraer, Y., Rabijns, A., Collet, J.F., Van Schaftingen, E. and De Ranter, C. (2004). How calcium inhibits the magnesium-dependent enzyme human phosphoserine phosphatase. *Eur J Biochem* 271, 3421-7.
- [45] Jun, Y.W., Hebenbrock, M. and Kool, E.T. (2019). A fluorescent hydrazone exchange probe of pyridoxal phosphate for the assessment of vitamin B6 status. *Chem Commun (Camb)* 56, 317-320.
- [46] Jeanclos, E.M., Lin, L., Treuil, M.W., Rao, J., DeCoster, M.A. and Anand, R. (2001). The chaperone protein 14-3-3eta interacts with the nicotinic acetylcholine receptor alpha 4 subunit. Evidence for a dynamic role in subunit stabilization. *J Biol Chem* 276, 28281-90.
- [47] Laskowski, R.A., Jablonska, J., Pravda, L., Varekova, R.S. and Thornton, J.M. (2018). PDBsum: Structural summaries of PDB entries. *Protein Sci* 27, 129-134.
- [48] Eisenberg, D., Schwarz, E., Komaromy, M. and Wall, R. (1984). Analysis of membrane and surface protein sequences with the hydrophobic moment plot. *J Mol Biol* 179, 125-42.

## **ACKNOWLEDGMENTS**

We thank Beate Vogt and Angelika Keller for excellent technical assistance.

## **CONFLICT OF INTEREST**

The authors declare that they have no conflicts of interest with the contents of this article.

## **FINANCIAL DISCLOSURE**

This work was supported by the Medical Faculty of the University of Düsseldorf (Grant 9772254 to A.G.), the Deutsche Forschungsgemeinschaft (SFB728 and SFB688 to A.G.), and by the Rudolf Virchow Center (FZ 82 to A.G. and H.S.). G.K. was supported by a Career Development Fellowship from the Graduate School of Life Sciences of the University of Würzburg.

## **AUTHOR CONTRIBUTIONS**

Conceived and designed experiments: E.J., G.K., H.S., A.G. Performed experiments: E.J., G.K., A.H., O.F., A.O., A-K.L. Analyzed the data: E.J., G.K., A.G. Wrote the paper: A.G.

## FIGURE LEGENDS

### Figure 1. Identification of CIB1 as a PDXP interactor

(A) Yeast two-hybrid assays. Protein-protein interactions are shown by  $\beta$ -galactosidase activity (blue) in streaks of yeast cells on a culture plate with selection medium. Yeast viability is documented on a culture plate with growth medium. (B) Solid phase binding assays. Immobilized, untagged CIB1 was incubated with the indicated amounts of PDXP, and binding was detected with PDXP-specific antibodies. Results are mean values  $\pm$  SD;  $n=3$ . The purity of CIB1 and PDXP ( $\sim 3$   $\mu\text{g}/\text{lane}$ ) is shown in the Coomassie Blue-stained gel in the inset. (C) GST pulldown assays. Purified PDXP (top), lysates of HeLa cells expressing myc-PDXP (middle), or mouse brain lysates (bottom) were incubated with  $\sim 5$   $\mu\text{g}$  immobilized GST-CIB1 or the GST control (comparable loading is shown on the Ponceau S-stained membranes), and bound PDXP was detected by immunoblotting. In the top and bottom panels, GST-CIB1 pulldowns were performed in duplicates. The concentrations of protein inputs for pulldowns/positive controls were: 5  $\mu\text{g}/15$  ng purified PDXP, and 300  $\mu\text{g}/20$  (10)  $\mu\text{g}$  HeLa cell (mouse brain) lysates ( $n \geq 3$ ). (D) Co-immunoprecipitation experiments. CIB1 was immunoprecipitated from HEK293 cells expressing untagged PDXP and/or untagged CIB1, and PDXP and CIB1 were detected by immunoblotting ( $n=3$ ). (E, F) GST pulldown assays. (E) HEK293 cells expressing GST or GST-PDXP together with untagged CIB1 were treated with 20  $\mu\text{M}$  of the  $\text{Ca}^{2+}$ -chelator BAPTA-AM (+) or with the vehicle DMSO (-) for 30 min. GST-pulldowns and the corresponding cell lysates were probed with  $\alpha$ -PDXP and  $\alpha$ -CIB1 antibodies. Note that the upper band in the CIB1 immunoblot of the pulldowns is non-specific. (F) As in (E), but HEK293 cells were treated with 5  $\mu\text{M}$  of the  $\text{Ca}^{2+}$ -ionophore A23187 (+) or with the vehicle DMSO (-) for 3 min. ( $n=3$ ).

### Figure 2. Mapping of the CIB1 binding site on PDXP

(A) Secondary structure plot for murine PDXP (PDB entry 4BX3), generated by PDBsum [47]. The PDXP N-terminus comprising amino acids (a.a.) 1-126 is shown enlarged below the full-length structure plot. Helices are labeled H1-H14, and  $\beta$ -strands are labeled A-D according to the  $\beta$ -sheet they belong to. Motifs:  $\beta$ , beta turn;  $\gamma$ , gamma turn; , beta hairpin. , Disulphide bond. Residue contacts: , to ligand; , to metal. The position of the active site motifs I and II is indicated below the amino acid sequence of the enlarged structure plot. The thick blue lines

represent the generated PDXP constructs that were tested in **(B)**; numbers indicate amino acids. **(B)** Interaction site mapping in yeast. Full-length murine PDXP or truncation mutants were co-transformed with murine CIB1. For each condition, replicates of three different yeast colonies plated on growth or selection medium are shown. **(C)** CIB1 binding site on PDXP (PDB entry 4BX3). Light grey, PDXP catalytic core domain; dark grey, capping domain; red, CIB1 binding site (a.a. 75-85). The active site with bound  $Mg^{2+}$  (green sphere) is marked by a green arrow. **(D)** Solid phase binding assays. Increasing concentrations of the PDXP<sup>76-90</sup> peptide, but not of a scrambled peptide, compete with PDXP binding to immobilized CIB1. The PDXP<sup>76-90</sup> peptide does not inhibit the CIB1-PAK1 interaction, which was tested in the presence of 100  $\mu$ M added  $Ca^{2+}$ . Please note that the fourth data point for the CIB1-PAK1 experiment corresponds to a molar ratio of 1:1600. Data are mean values  $\pm$  SD,  $n=3$ .

### Figure 3. Mapping of the PDXP binding site on CIB1

**(A)** Hydrophobic channel in CIB1 (PDB entry 1XO5). Residues are colored according to the Eisenberg hydrophobicity scale [48]. Red, hydrophobic; white, hydrophilic. The position of helix 10 (H10) is indicated in the surface (upper) and the corresponding cartoon representation of CIB1 (lower). **(B)** Secondary structure plot for human CIB1 (PDB entry 1XO5), generated by PDBsum. The CIB1 C-terminus comprising amino acids (a.a.) 99-191 is shown enlarged below the full-length structure plot. Helices are labeled H1-H13, and the strands of the beta sheet are labeled as A. Motifs:  $\beta$ , beta turn;  $\gamma$ , gamma turn;  $\equiv$ , beta hairpin. Residue contacts to metal:  $\blacksquare$ . The position of EF-hands III and IV is indicated. The thick blue lines represent the CIB1 constructs that were tested in **(C)**; numbers indicate amino acids. **(C)** Mapping of the PDXP-binding site on CIB1 in yeast. The indicated CIB1 constructs were co-transformed with PDXP<sup>wt</sup>. Control, pB42AD vector. **(D)** Solid phase binding assays. PDXP binding to immobilized CIB1<sup>wt</sup> or CIB1<sup>1-173</sup> was assessed. Results are mean values  $\pm$  SD,  $n=3$ . Protein purities are shown in the Coomassie Blue-stained gel. **(E)** PDXP binding site on CIB1 (PDB entry 1XO5). Amino acids 173-191 of CIB1 are marked in red.

### Figure 4. Identification of CaM as a PDXP and CIB1 binding partner

Pulldown binding assays with immobilized CaM. **(A)** Purified PDXP and/or CIB1 (molar ratio PDXP:CIB1=1:10) were incubated with CaM-sepharose or sepharose control beads. Bead-associated PDXP and CIB1 were detected by immunoblotting. The input is a fraction of the PDXP

+ CIB1 mixture. Note that excess CIB1 competes with PDXP binding to CaM (compare lanes 3 and 7). **(B)** Rat testis whole cell lysates (WCL) were incubated with either CaM-sepharose or control beads. **(C)** Effect of added  $\text{Ca}^{2+}$  on the association of purified PDXP and CIB1 with CaM. Note that the  $\text{Ca}^{2+}$ -dependent increase of PDXP binding to CaM occurs even in the presence of a 10-fold molar excess of CIB1 (compare lanes 1 and 2 with lanes 5 and 6). **(D)** The PDXP<sup>76-90</sup> peptide competes with PDXP binding to CaM-sepharose. All blots are representative of  $n=3$  experiments.

### **Figure 5. $\text{Ca}^{2+}$ regulates PDXP complex formation with CIB1 or CaM**

Crosslinking experiments with purified, untagged PDXP (5  $\mu\text{M}$ ), CIB1 and CaM (10  $\mu\text{M}$  each) were performed using 0.67% formaldehyde. **(A)** *Left panel*, Crosslinking experiments in the absence or presence of  $\sim 25 \mu\text{M}$   $\text{Ca}^{2+}$ . Proteins were separated on a 12% SDS-PAGE gel and stained with Coomassie Brilliant Blue. MWM, molecular weight marker. The positions of the individual proteins and protein complexes are indicated. *Right panel*, Densitometric analysis of PDXP-CIB1 and PDXP-CaM complexes when crosslinking reactions were performed with PDXP and CIB1, or with PDXP and CaM. Data represent mean values  $\pm$  SEM;  $n=6$ . Differences were analyzed with the Mann-Whitney two-tailed test. **(B)** Effect of different  $[\text{Ca}^{2+}]$  on crosslinking efficiencies. *Left panel*, Proteins were resolved on a 15% SDS-PAGE gel and stained with Coomassie Brilliant Blue. Note that CaM migrates as multiple bands at low  $[\text{Ca}^{2+}]$ . *Right panel*, Densitometric analysis of PDXP-CIB1 and PDXP-CaM complex formation when crosslinking reactions were performed with PDXP, CIB1 and CaM. The total complex formation represents the aggregate of the two binary complexes. To test for statistically significant differences, the effects of different  $[\text{Ca}^{2+}]$  on PDXP-CIB1 or PDXP-CaM complex formation were compared to the conditions without added  $[\text{Ca}^{2+}]$ . \*\*,  $p < 0.005$ ; \*,  $p < 0.05$ . Data are mean values  $\pm$  SEM;  $n=3$ .

### **Figure 6. Summary and model**

Identification of  $\text{Ca}^{2+}$ -dependent, binary protein-protein interactions between PDXP, CIB1 and calmodulin (CaM). The upper panels indicate the effects of  $\text{Ca}^{2+}$  on these interactions, and the lower panels illustrate the resulting protein complexes. **(A)** PDXP can bind CIB1 or CaM in a mutually exclusive manner. CIB1 and CaM can also interact. This can lead to the formation of three different protein-protein complexes (bottom panel). **(B)** Elevated  $[\text{Ca}^{2+}]$  trigger conformational changes in CIB1 and CaM (diamond shapes when  $\text{Ca}^{2+}$ -bound), and decrease the

CIB1-CaM association (dashed line). Increased  $\text{Ca}^{2+}$  levels promote CaM binding to PDXP (thick line), and competitively diminish CIB1 binding to PDXP, although the CIB1-PDXP association *per se* is not dependent on changes in  $[\text{Ca}^{2+}]$  (similar line strength in **A** and **B**). Hence,  $\text{Ca}^{2+}$  functions as a molecular switch that promotes CaM-PDXP complex formation, and CIB1-PDXP and  $\text{Ca}^{2+}$ -CaM-PDXP complexes may be functionally different.

**TABLE**

**Table 1: Effect of CIB1 or CaM on the catalytic constants of PDXP towards PLP**

	$K_m$ ( $\mu\text{M}$ )	$v_{\text{max}}$ ( $\mu\text{mol}/\text{min}/\text{mg}$ )	$k_{\text{cat}}$ ( $\text{s}^{-1}$ )	$k_{\text{cat}}/K_m$ ( $\text{s}^{-1} \text{M}^{-1}$ )	
1 mM EGTA	PDXP	$54.4 \pm 4.7$	$3.1 \pm 0.1$	$1.62 \pm 0.04$	$2.98 \times 10^4$
	PDXP + CIB1	$55.5 \pm 4.4$ (102%)	$2.9 \pm 0.1$ (94.5%)	$1.53 \pm 0.04$ (94.6%)	$2.76 \times 10^4$ (92.6%)
	PDXP + CaM	$50.9 \pm 3.2$ (93.6%)	$2.9 \pm 0.1$ (94.3%)	$1.53 \pm 0.03$ (94.4%)	$3.00 \times 10^4$ (100.7%)
100 $\mu\text{M}$ $\text{Ca}^{2+}$	PDXP	$76.4 \pm 3.0$	$2.8 \pm 0.04$	$1.51 \pm 0.02$	$1.97 \times 10^4$
	PDXP + CIB1	$82.1 \pm 5.0$ (107.6%)	$2.6 \pm 0.1$ (92.3%)	$1.39 \pm 0.03$ (92.3%)	$1.69 \times 10^4$ (85.8%)
	PDXP + CaM	$67.6 \pm 4.3$ (88.5%)	$2.6 \pm 0.1$ (91.6%)	$1.38 \pm 0.03$ (91.6%)	$2.04 \times 10^4$ (103.6%)

Kinetic constants of PDXP-catalyzed PLP hydrolysis in the absence or presence of either CIB1 or CaM under  $\text{Ca}^{2+}$ -free or  $\text{Ca}^{2+}$ -containing conditions. The data shown are mean values  $\pm$  SEM of three independent experiments each performed in triplicates, using three independently purified batches of proteins. The numbers in parentheses represent the relative values of the constants

compared to the respective values for PDXP alone.  $K_m$ , Michaelis-Menten constant;  $v_{max}$ , maximum enzyme velocity;  $k_{cat}$ , turnover number;  $k_{cat}/K_m$ , specificity constant.

Accepted Article

**Fig. 1**

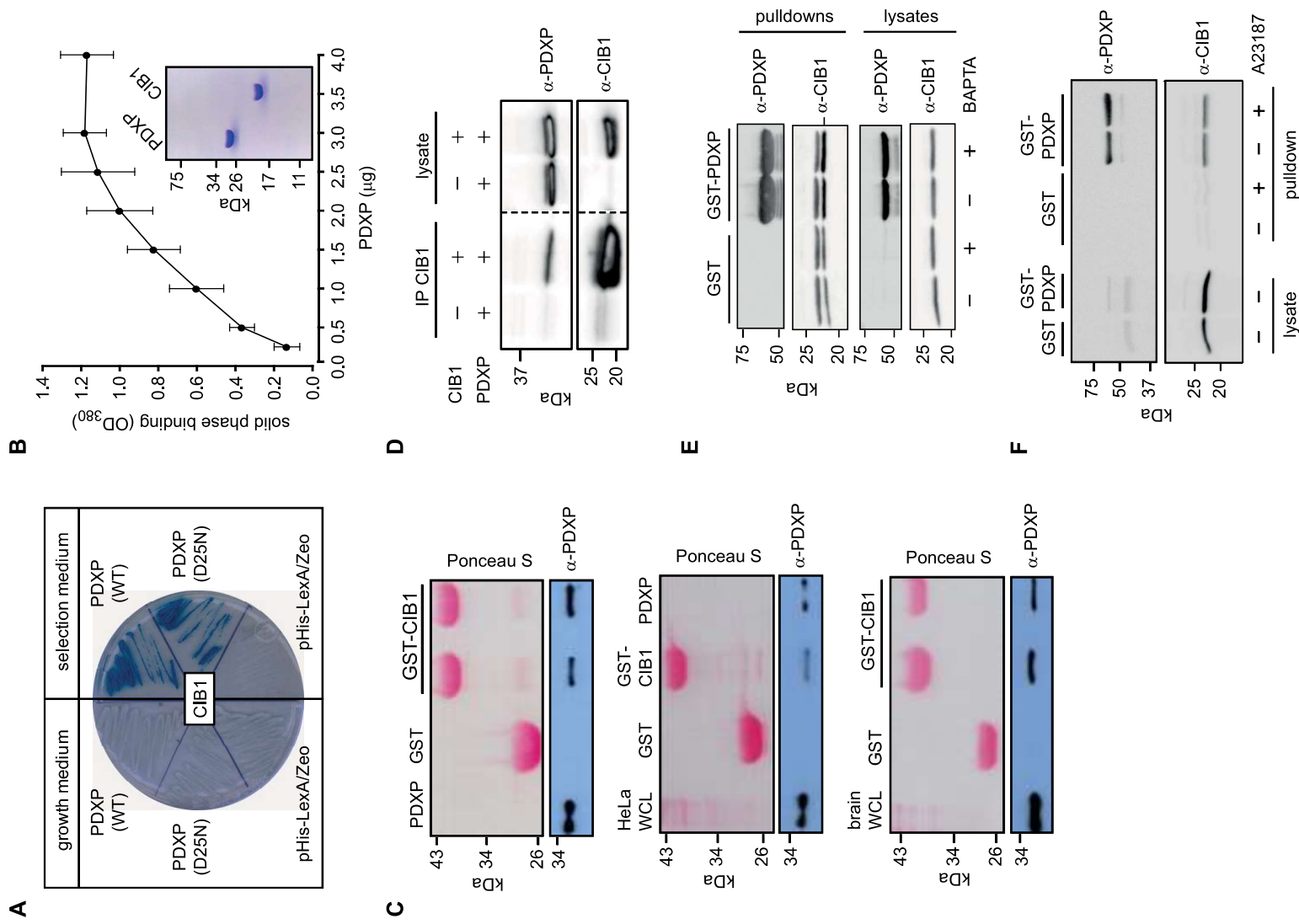
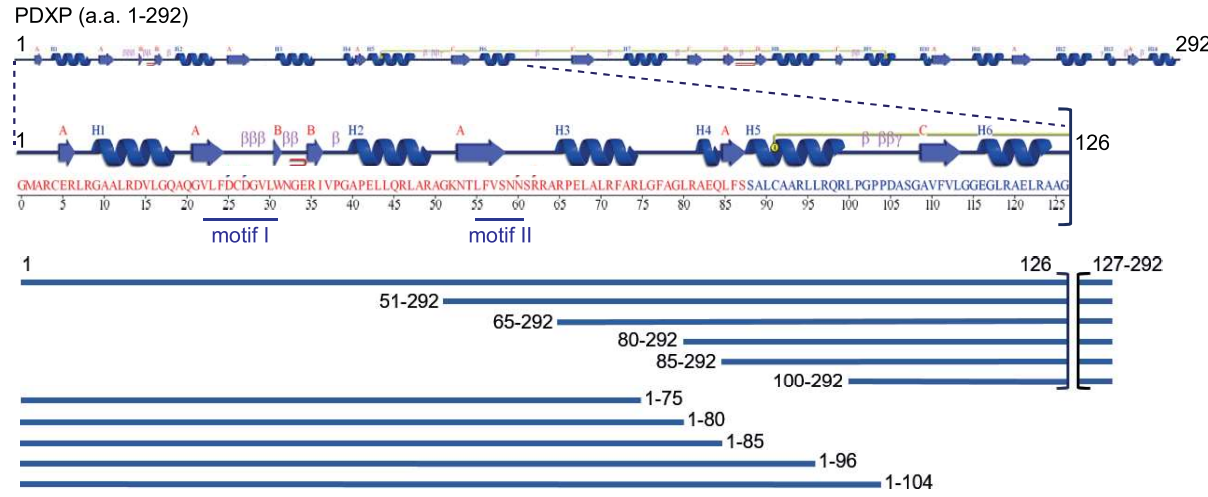
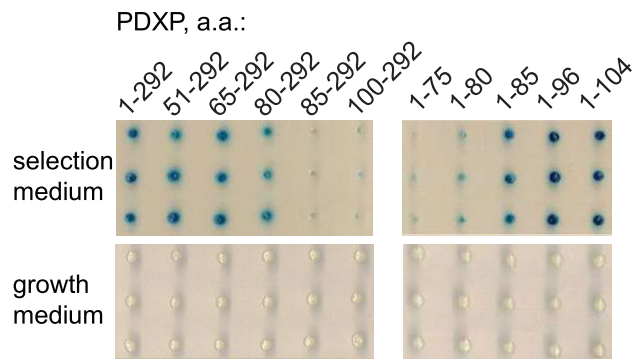


**Fig. 2**

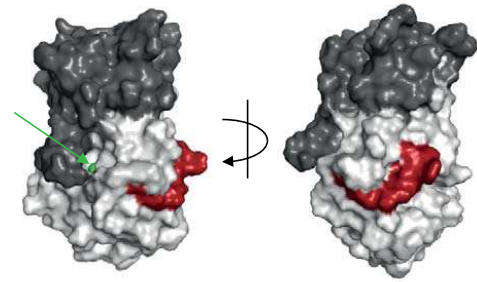
**A**



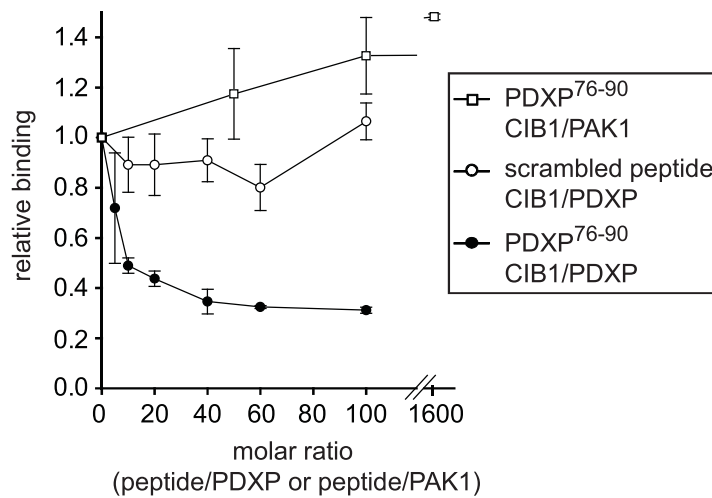
**B**

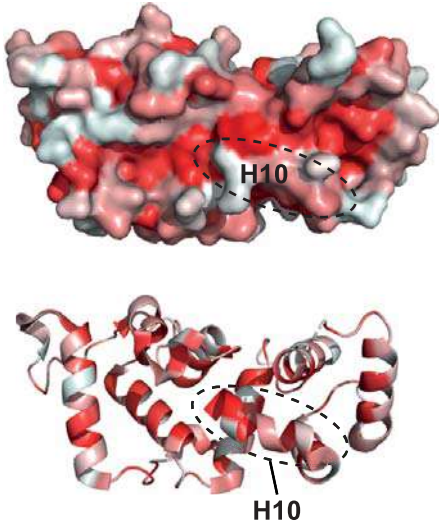
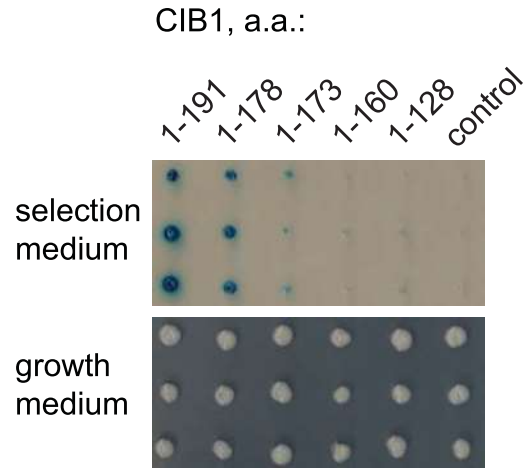
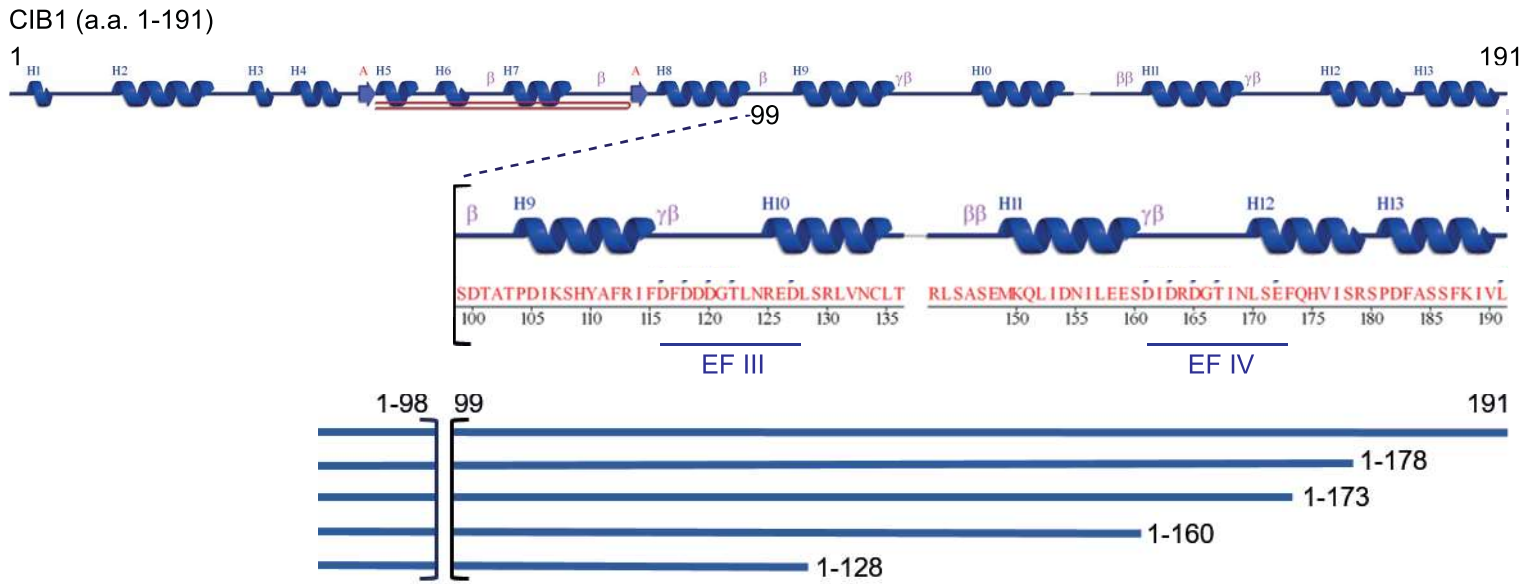
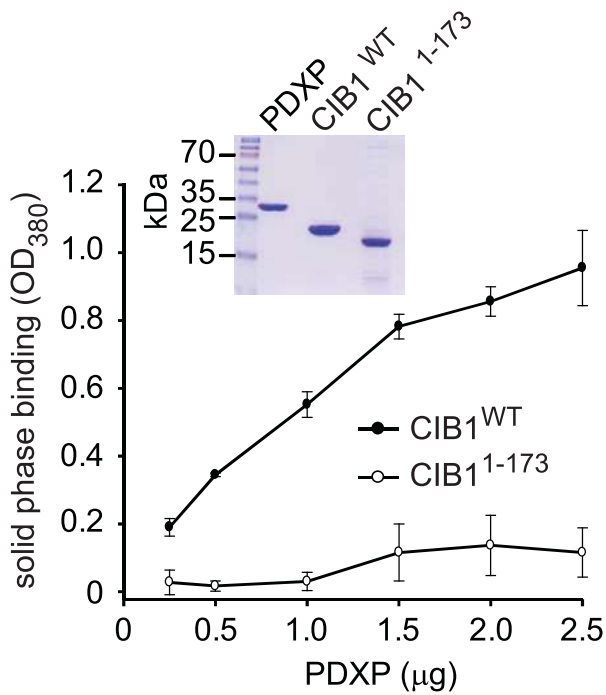
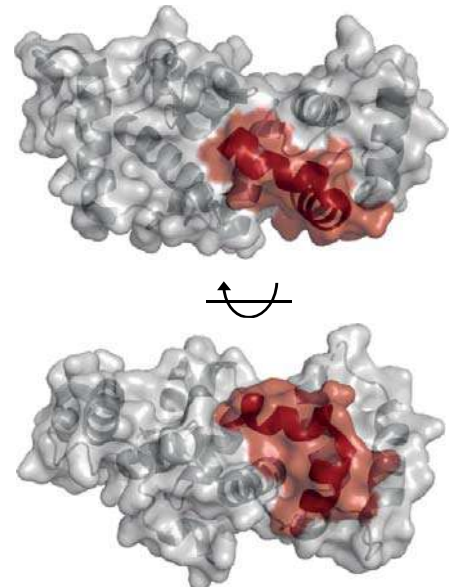


**C**



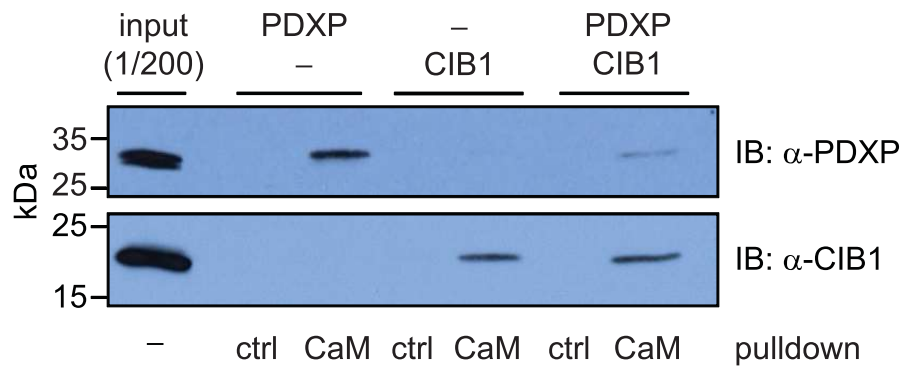
**D**



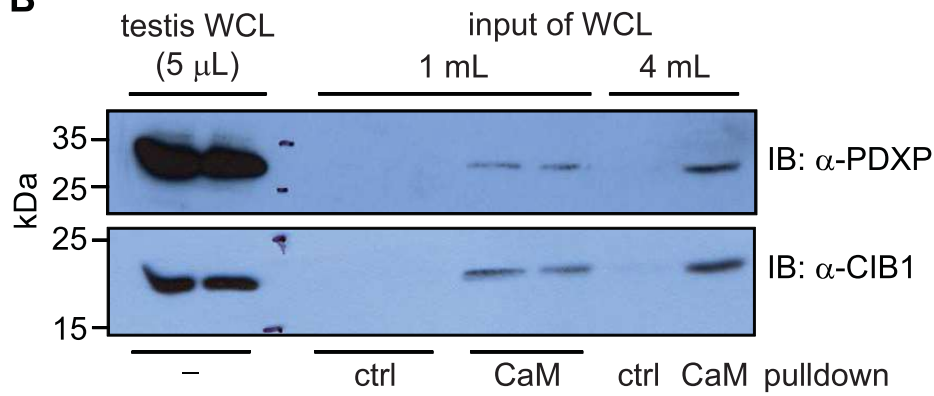
**Fig. 3****A****C****B****D****E**

**Fig. 4**

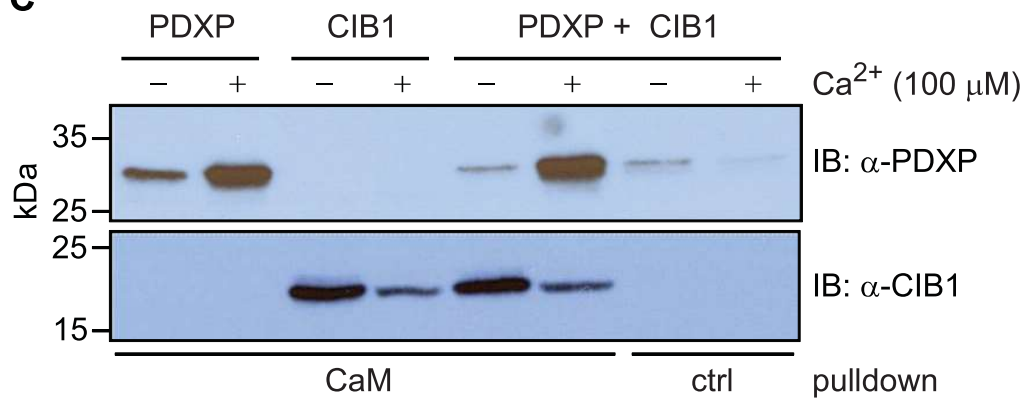
**A**



**B**



**C**



**D**

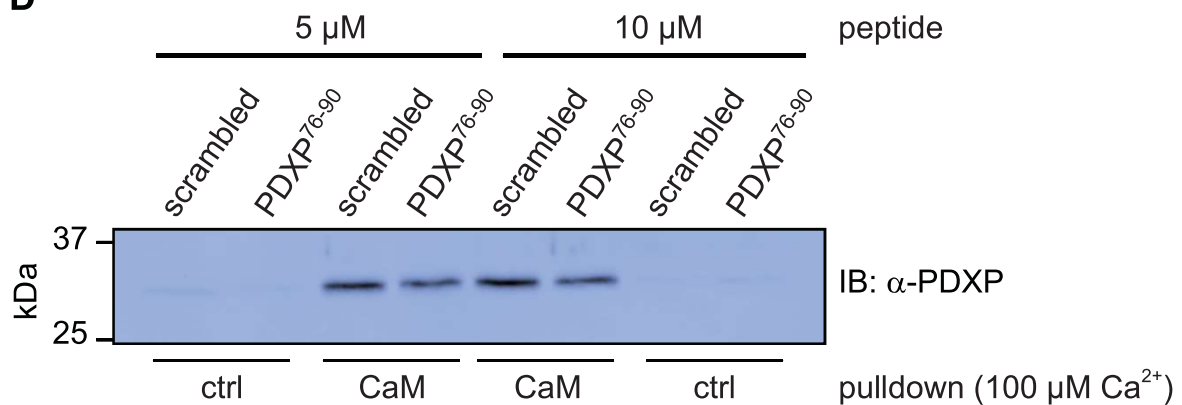


**Fig. 5**

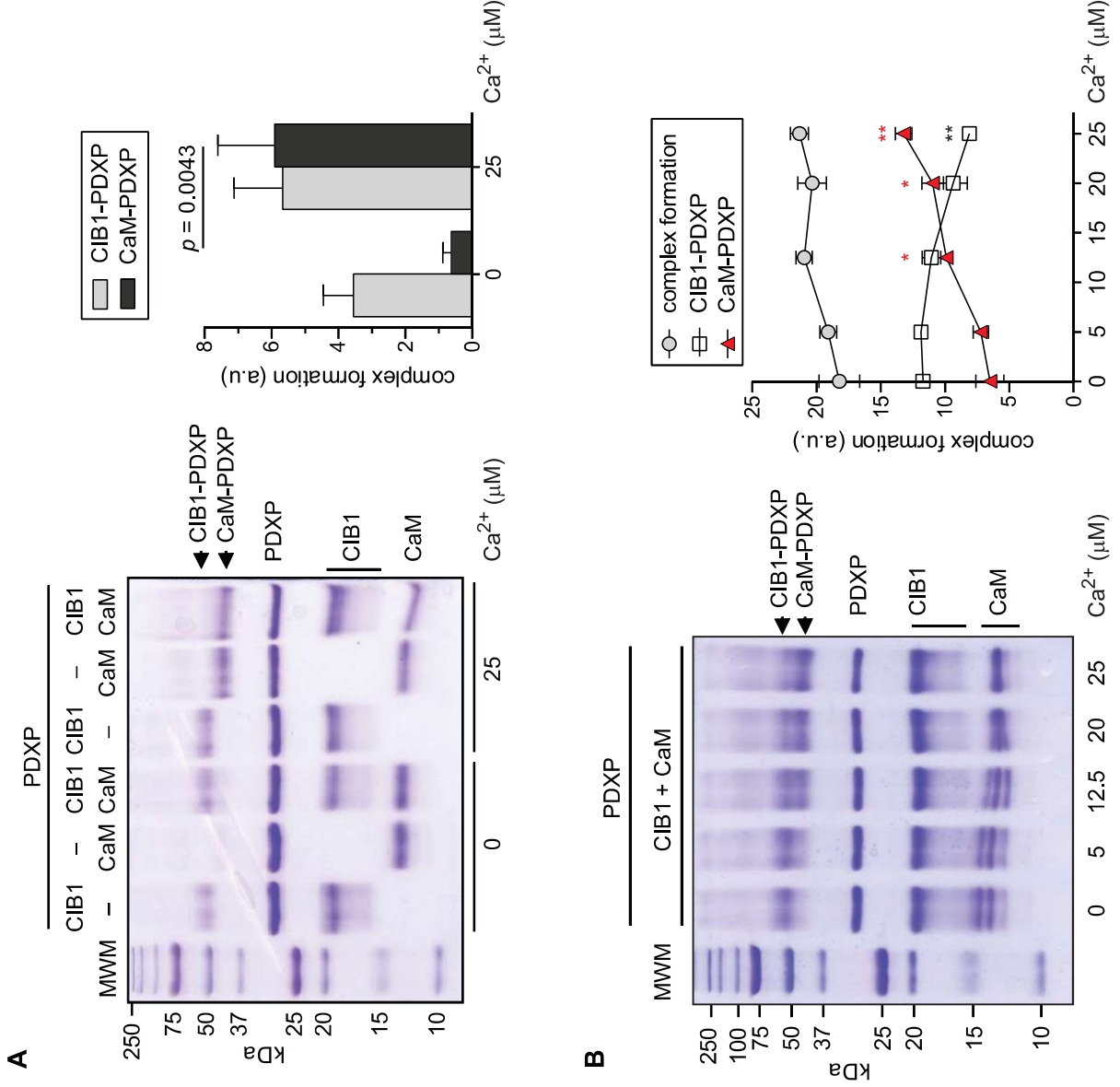
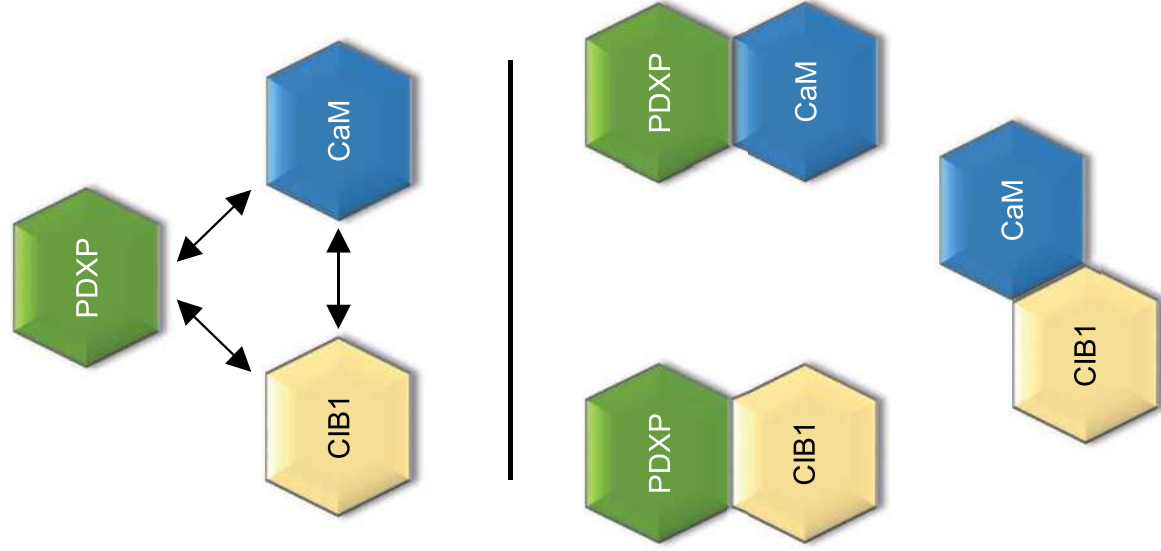


Fig. 6

A

basal  $[Ca^{2+}]$



B

elevated  $[Ca^{2+}]$

